Optical Materials 33 (2011) 1884–1891

Contents lists available at ScienceDirect

Optical Materials

journal homepage: www.elsevier.com/locate/optmat

Thermal precipitation of silver nanoparticles and thermoluminescence in tellurite glasses

J.M. Giehl [a,*], W.M. Pontuschka [a], L.C. Barbosa [b], E.F. Chillcce [b], Z.M. Da Costa [c], S. Alves [a,d]

[a] Instituto de Física da Universidade de São Paulo, Rua do Matão, 187 – Travessa R, 05508-090 São Paulo, SP, Brazil
[b] Laboratório de Materiais, UNICAMP, Box 6165, 13083-970 Campinas, SP, Brazil
[c] LaProMaV, Universidade Federal de Juiz de Fora, Juiz de Fora, MG 36036-330, Brazil
[d] Departamento de Ciências Exatas e da Terra, Universidade Federal de São Paulo, Diadema, São Paulo, Brazil

ARTICLE INFO

Article history:
Received 24 November 2010
Received in revised form 2 March 2011
Accepted 4 March 2011
Available online 31 March 2011

Keywords:
Tellurite glasses
Silver nanoparticles
Optical absorption
EPR
TL

ABSTRACT

Silver metal and/or oxide precipitation of nanoparticles in thermally treated Ag-doped tellurite glasses was studied by optical absorption (OA) and transmission electron microscopy (TEM). The Lorentzian adjusted silver nanoparticles plasma resonance OA band was compared to the Drude model approach. The silver nanoparticles size distribution on the surface rather than in the bulk was determined by TEM. A model for the metallic silver precipitation is proposed. The characterization of the formation of silver nanoparticles was carried out with differential thermal analysis (DTA) to determine the glass transition temperature (Tg) and of crystallization (Tc). Previously γ-irradiated samples exhibited thermoluminescence (TL) peaks and the defect centers TeOHC, NBOHC and TeEC were identified by electron paramagnetic resonance (EPR), but no Ag^0 signal was detected. The silver nanoparticles are known to introduce desired third-order optical nonlinearities in the composites, at wavelengths close to the characteristic surface-plasmon resonance of the metal precipitates. An increase of the glass density and refractive index with increasing $AgNO_3$ content was observed.

1. Introduction

The tellurite glasses have a great potential for applications in fast optical switching, lasers of nonconventional luminescence, optical fiber amplifier light sources for applications in broad band telecommunications in the range about 1.5 μm [1–3]. Recent studies dealing with phenomena involved with TL, OA and infrared in TeO_2 glasses have been reported [4–6]. However, compared with the better nonlinear properties of the optical crystals and polymers, the nonlinearity of the conventional tellurite glasses is still unsatisfactory. The applications in devices which demand strong luminescence are accomplished with heavy metal oxide (HMO) glasses doped with trivalent rare earth ions due to their small cutoff phonon frequencies [7,8]. The use of silver as a luminescence sensitizer of rare earth ions in the glasses is encouraged because the small absorption cross sections have afforded the attempts to increase the excitation efficiency of these ions [9,10].

The aim of the present paper is to study the silver nanoparticle size evolution with the thermal treatment (TT) temperature via TEM and OA. Another objective is the development investigations of the possible metallic silver precipitation produced by the exposure to gamma irradiation and to study the defect structures with the aid of EPR and TL. There is still a lack of more detailed models to explain the conditions and mechanisms of the precipitation and dilution of silver nanoparticles in tellurite glasses, justifying the need of more research work in this area.

2. Experimental

The glass samples were prepared by melt-quenching method using appropriately weighed high-purity compounds: TeO_2 (99.999%), Na_2CO_3 (99.995%), ZnO (99.99%) and $AgNO_3$ (99.9999%). The batches were held at the temperature of 850 °C at an electric furnace, in air, during 30 min in platinum crucible. In Table 1 the nominal sample compositions are shown.

The thermograms of the differential thermal analysis (DTA) were obtained with the model DTA-50 of Shimatzu equipment. Two platinum crucibles of dimensions 5.6 mm of diameter and 2.5 mm height were used and care was taken in order to prevent contamination. The DTA measurements required two crucibles: one empty and another containing the sewed powdered glass sample of average grain diameter of 75 μm weighing about 40 mg and the heating rate was 10 °C/s. The values of glass transition (Tg) crystallization (Tc) and melting (Tm) temperatures are shown in Table 1.

* Corresponding author.
E-mail address: juliagiehl@hotmail.com (J.M. Giehl).

0925-3467/$ - see front matter Crown Copyright © 2011 Published by Elsevier B.V. All rights reserved.
doi:10.1016/j.optmat.2011.03.006

Table 1
Nominal compositions and glass transition (Tg), crystallization (Tc) and melting (Tm) temperatures.

Sample	Composition (mol%)	Dopant (mol%)	Tg (°C)	Tc (°C)	Tm (°C)
B_1	(60 TeO_2·25 ZnO·15 Na_2O)	None	256	404	490
B_2	(60 TeO_2·25 ZnO·15 Na_2O)	0.5	256	417	491
B_3	(60 TeO_2·25 ZnO·15 Na_2O)	5	243	368	485

The optical absorption (OA) were performed with the model 500 double-beam Cary spectrophotometer in the absorbance mode, in the wavelength range of 200–3000 nm.

The morphology of the precipitated nanoparticles was studied with the aid of the transmission electron microscope (TEM) Philips model CM 200, operating at 200 kV.

The samples were γ-irradiated at room temperature using Panoramic 60Co cobalt source at the conditions given in Table 2.

The EPR spectra were taken at Bruker homodyne X-band spectrometer. In order to avoid the systematic error in the g values the magnetic field correction was determined using a standard sample of DPPH ($g = 2.0036 \pm 0.0002$). The uncertainties were calculated by the error propagation method, starting from the magnetic field uncertainty.

The TL emission curves were obtained using a Daybreak-type reader 1100 Automated TL System.

A complementary determination of some important additional physical properties for an adequate characterization of the glass samples included the linear refraction indices at different wavelengths and densities.

The refractive indices were performed at room temperature (~300 K) using the Metricon Model 2010 equipament containing three laser light sources of wavelengths 632.8, 1305 and 1536 nm, respectively, which allows the refractive indices measurements with precision of 0.0002.

The densities were determined using the Archimedes method, with precision of 0.0001 g, with distilled water as the immersion fluid.

3. Results

3.1. Linear refractive index

The values of the densities and refractive indices at the wavelengths of 632.8, 1305.4 and 1536 nm of the samples B_1, B_2 and B_3 are shown in Table 3. It is seen that the densities and refractive indices increase with increasing the $AgNO_3$ content.

3.2. Optical absorption (OA)

With the objective to investigate a possible precipitation of metallic silver nanoparticles, we decided to carry out a set of thermal treatments (TT).

Table 2
Irradiation doses.

Samples	Dose (kGy)	Dose rate (kGy/h)	Distance (cm)	Time of exposition (min)
B_1, B_2, B_3	1	0.1862	10.0 (0.1)	322.2
B_1	5	0.3622	5.0 (0.1)	828

Table 3
Densities and linear refractive index.

Sample	Densities (g/cm^3)	Refractive index		
		632.8	1305.4	1536
B_1	4.8840 ± 0.0007	1.9093 ± 0.0005	1.8712 ± 0.0005	1.8668 ± 0.0005
B_2	4.9960 ± 0.0007	1.9119 ± 0.0005	1.8727 ± 0.0005	1.8681 ± 0.0005
B_3	5.1200 ± 0.0007	2.0138 ± 0.0005	1.9626 ± 0.0005	1.9370 ± 0.0005

The samples B_1, B_2 and B_3 do not present any OA band prior to the TT (Fig. 1). The samples were treated thermally at temperatures above Tg without applying a special atmosphere.

In the OA spectra of the sample B_2 of lower silver content (see Fig. 2) it is observed an increase of the silver plasmon resonance band intensity indicating an increasing number of silver nanoparticles after the thermal treatments (TT) at 270 °C, 290 °C and 310 °C for 2 h and a red shift from 446 nm to 455 nm and 466 nm, whereas the bandwidth (full width at half maximum (FWHM)) decreased from (117 ± 1) nm to (99 ± 9) nm and (63.7 ± 1,5) nm (see Table 4). This behavior is consistent with the nucleation and further growth of the nanoparticles [11]. For the sample B_3 (see Fig. 2) of higher silver content, the TT at 270 °C and 290 °C for 2 h produced a slight reduction of the peak intensity and therefore, of the number of particles, indicating a dissolution or either a clustering already at this TT stage. A red shift for TT from 270 °C to 290 °C a reduction in bandwidth from (178 ± 3) nm to (161 ± 7) nm is observed (see Table 4).

After the thermally treated sample was polished, the OA of the 480 nm band has disappeared (see Fig. 3), showing the evidence that the nucleation has occurred on the sample B_3 surface.

The silver doped samples of series B of the gap energy (E_{opt}) and Urbach energy are indicated in Table 5. The series B samples present a small difference in the optical gap energy (E_{opt}) showing that the silver addition to the composition decreases its magnitude in the sample B_3, in agreement with the similar behavior observed by Terashima et al. [12] in the B_2O_3–Ag_2O glass system.

3.3. Transmission electron microscopy (TEM) and X-ray fluorescence by energy dispersive spectroscopy (EDS)

The micrographs of the molten bulk samples were not useful for the silver nanoparticles analysis, so that the silver containing samples were sanded and the nanoparticles were successfully studied by TEM. Fig. 4 shows that the shape of the particles is approximately spherical, consistent with the corresponding Plasmon

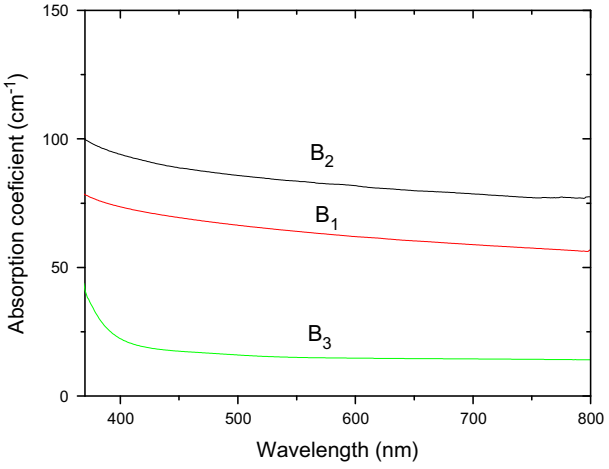

Fig. 1. OA spectra of the B_1, B_2 and B_3 without TT.

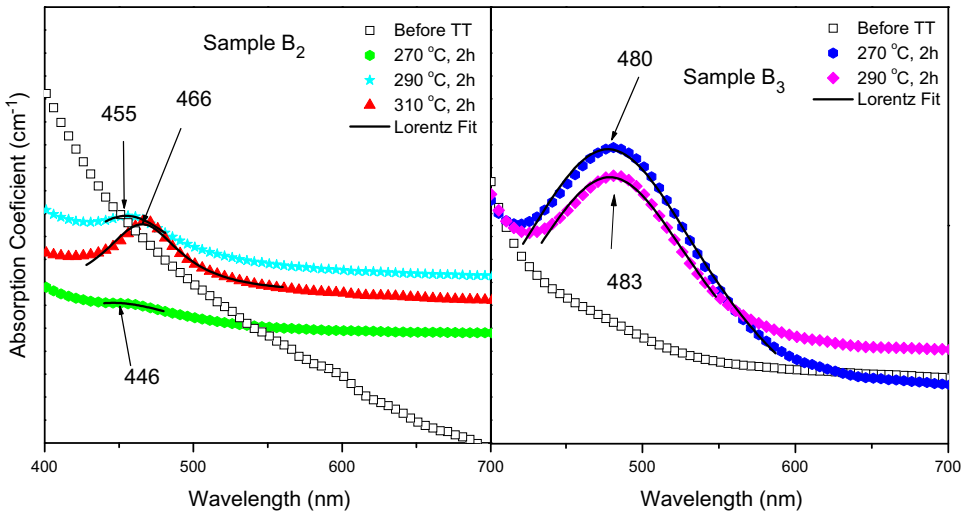

Fig. 2. OA spectra of the B_2 and B_3 samples as prepared with different TT's.

Table 4
Values of FWHM of B_2 and B_3 treated at different temperatures (see Fig. 2).

Sample	Temperature (°C)	FWHM
B_2	270	117 ± 18
	290	98 ± 9
	310	63.7 ± 1.5
B_3	270	178 ± 3
	290	161 ± 7

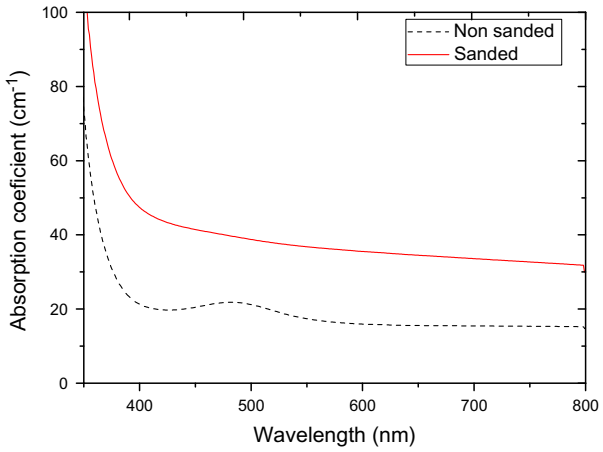

Fig. 3. Spectra B_3 sample sanded after TT.

Table 5
Optical gap and Urbach energies of the series B samples.

Sample	E_g (d.t.) (eV)	E_g (i.t.) (eV)	UE (meV)
B_1	3.34 ± 0.03	3.59 ± 0.03	192 ± 4
B_2	3.63 ± 0.03	3.83 ± 0.03	146.0 ± 2.0
B_3	2.40 ± 0.03	2.66 ± 0.03	330 ± 4

resonance wavelengths observed at 450, 456 and 468 nm, respectively, shown in Fig. 2 to left. The size of the nearly spherical nanoparticles precipitated at the surface of the B_2 sample, thermally treated at 270 °C for 2 h (see Fig. 4 to left) varied from 0.5 to 8 nm with the average diameter of (5 ± 1) nm. This micrograph shows that the nanoparticles were grown not embedded in the glass matrix. After the subsequent thermal treatment at 290 °C for 2 h the micrograph in Fig. 4 (to center) the average diameter of the nanoparticles scattered on the glass surface is (7 ± 1) nm of sizes between 0.5 and 10 nm. The next thermal treatment, at 310 °C for 2 h, (see Fig. 4 to right) yielded nanoparticles of average diameter (13 ± 1) nm with the size distributed between 4 and 26 nm.

Fig. 5 shows the energy dispersive spectrum (EDS) of the sample B_2 treated at 270 °C for 2 h. There are seen the peaks of the silver nanoparticles, ZnK and oxygen. The small Te amount means that the surface silver nanoparticles were found practically isolated from the glass matrix.

The TEM sample B_3, doped with 5 mol% of $AgNO_3$, thermally treated at 270 °C for 2 h (see Fig. 6 to left) exhibited nearly spherical nanoparticles of average diameter (9 ± 1) nm, which appeared either scattered or gathered in agglomerates. Further thermal treatment at 290 °C for 2 h there were observed particles and agglomerates of average particle size of (17 ± 1) nm (see Fig. 6 to right). No particles were found embedded in the sample B_3 glass matrix (the dark portion of the micrograph).

3.4. Electron paramagnetic resonance

The paramagnetic responses of γ-irradiated tellurite glasses were detected and interpreted: (a) a shoulder at $g_n = g_1 = 2.02 \pm 0.01$ of line-width $\Delta H_{pp} = (1.5 \pm 0.5)G$ and an underlying wing of estimated $g_\perp \sim 2.0$ ascribed to the tellurium–oxygen hole center (TeOHC); (b) a narrow line at $g_2 = 1.9960 \pm 0.0005$ of line-width $\Delta H_{pp} = (1.5 \pm 0.5)G$ ascribed to the non-bridging oxygen hole center (NBOHC) and (c) $g_3 = 1.9700 \pm 0.0005$ of $\Delta H_{pp} = (1.9 \pm 0.5)G$ due to the tellurium electron center (TeEC), respectively, shown in Fig. 7 [13].

Aiming a better understanding of the thermal behavior of the defect states in the tellurite glass, a set of EPR measurements was carried out to measure the isochronal thermal decay and resonances were recently attributed by Giehl et al. [13] Fig. 7 to the tellurium-oxygen hole center (TeOHC), non-bridging oxygen hole center (NBOHC), and tellurium electron center (TeEC), respectively.

With the objective to observe the thermal decay behavior of the EPR intensities of the resonances g_1, g_2 and g_3, as well as the temperature limit where the defect centers are extinguished, the isochronal curves were constructed of the samples B_1, B_2 and B_3

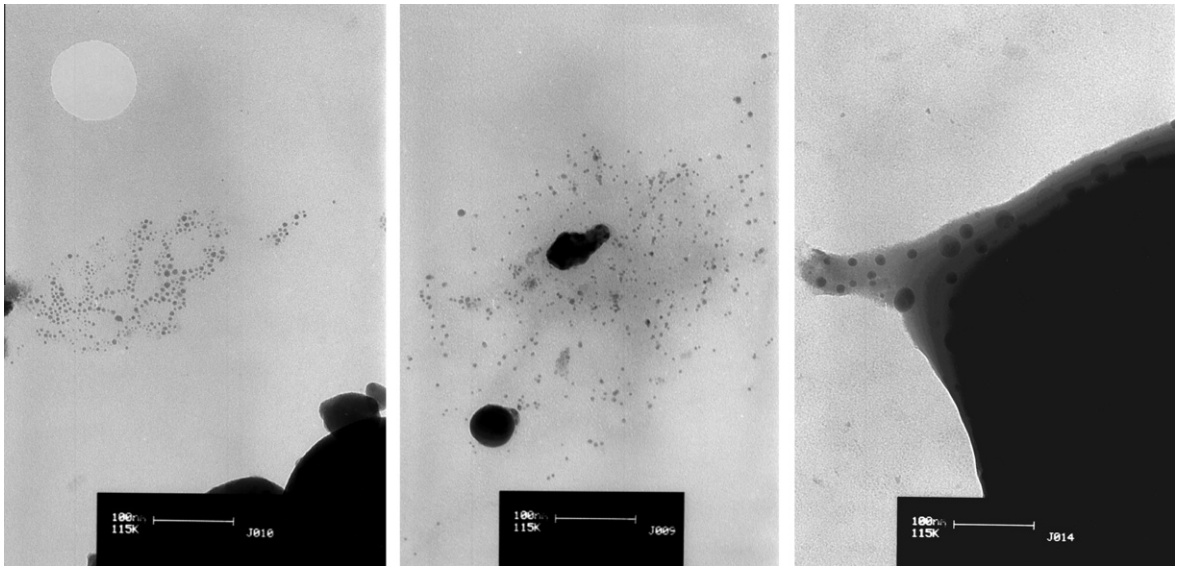

Fig. 4. TEM micrographs of the sample B_2 after TT at 270 °C for 2 h (left) at 290 °C (center) and at 310 °C (right) for 2 h.

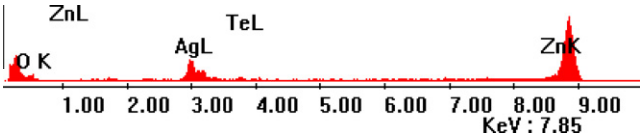

Fig. 5. EDS spectrum of the sample B_2 after TT at 270 °C for 2 h.

gamma irradiated with dose of 1 kGy and thermally treated during 10 min for each temperature. The relative intensity versus temperature were plotted for the samples B_1, B_2 and B_3 is shown in Figs. 8–10. A common characteristic of all the curves is that the g_1 resonance is not completely extinguished up to the temperature of 140 °C.

In sample B_1, the g_2 and g_3 resonances are completely bleached at the temperatures of 140 °C and 160 °C, respectively, whereas for the samples B_2 and B_3 (see Figs. 9 and 10) the resonances g_2 and g_3 are completely extinguished at 160 °C.

3.5. Thermoluminescence

The TL curves of B_1, B_2 and B_3 samples were measured immediately after irradiation of dose 1 kGy, shown in Figs. 11–13, respectively. The activation energies of the TL initial slope are given in Table 6. The TL peak values of each sample were obtained from the Gaussian adjustments and are shown in Table 6.

4. Discussion

From the measured values of density and refractive index of the samples B_1, B_2 and B_3 it is easily verified that the silver doping has not affected the molar volume of the glass, so that the increase in the refractive index is due merely to the heavier atomic weight of silver added ions and thus no significant structural changes have been occurred.

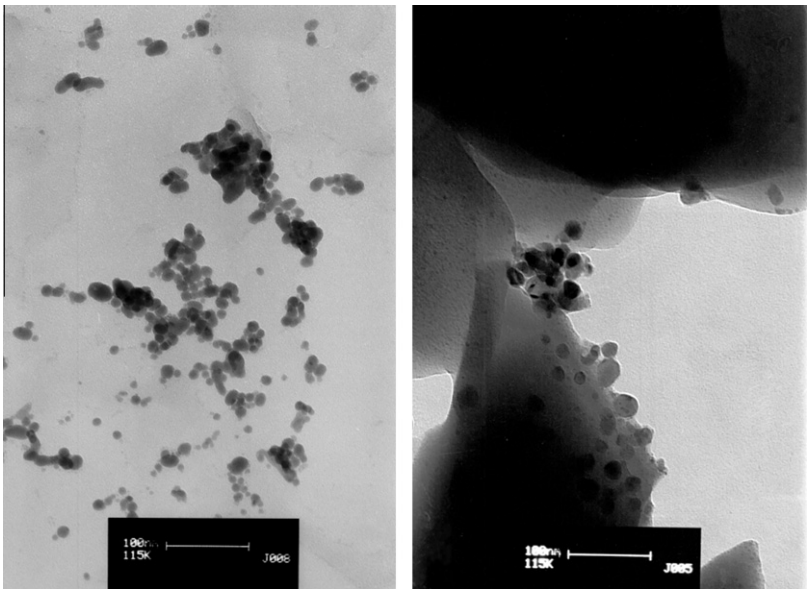

Fig. 6. TEM micrographs of the sample B_3 after TT at 270 °C (left) and 290 °C (right) after 2 h.

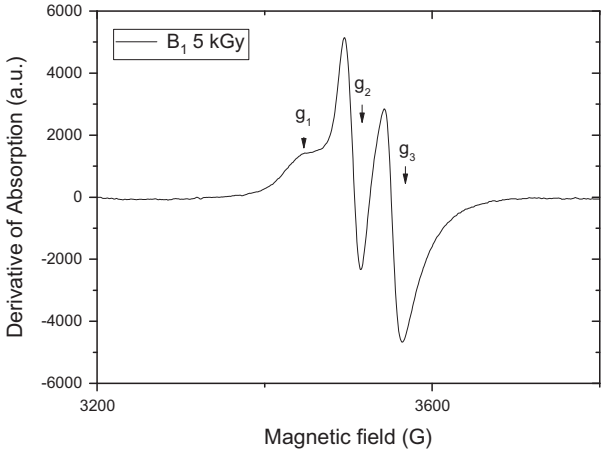

Fig. 7. Paramagnetic responses of γ-irradiated tellurite glasses [13].

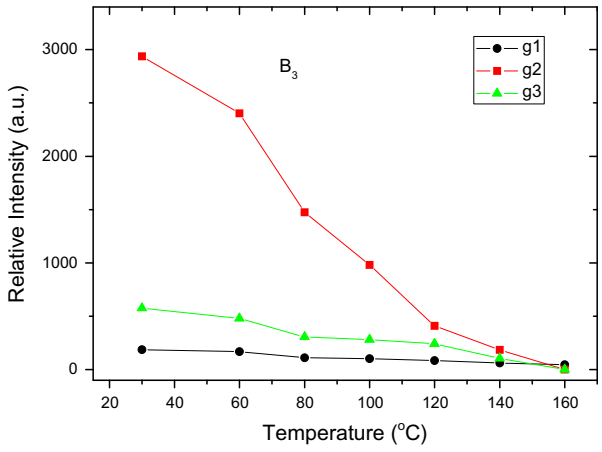

Fig. 10. Isochronal thermal treatment curve of the sample B_3 EPR responses.

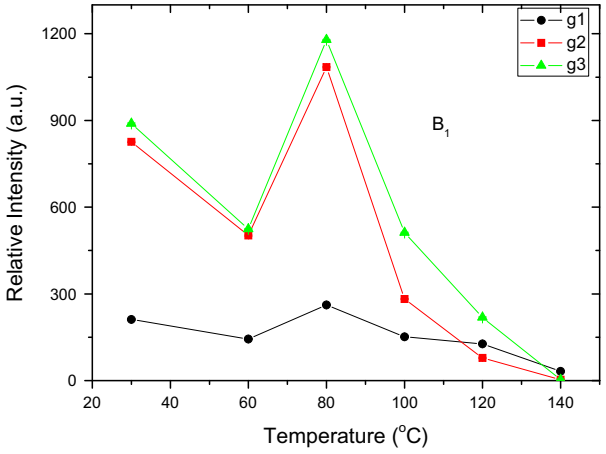

Fig. 8. Isochronal thermal treatment curve of the sample B_1 EPR responses.

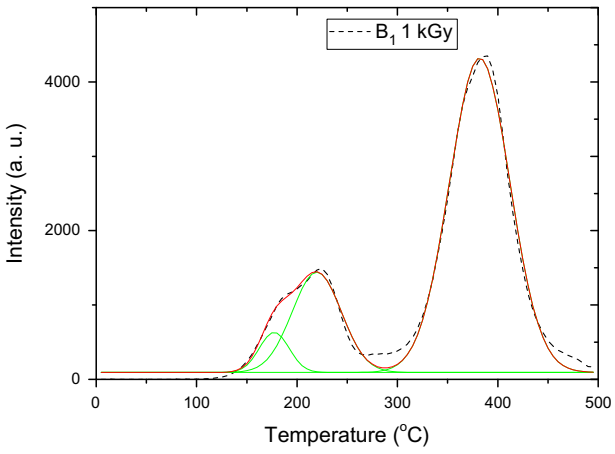

Fig. 11. TL glow curve of the sample B_1 irradiated with dose 1 kGy.

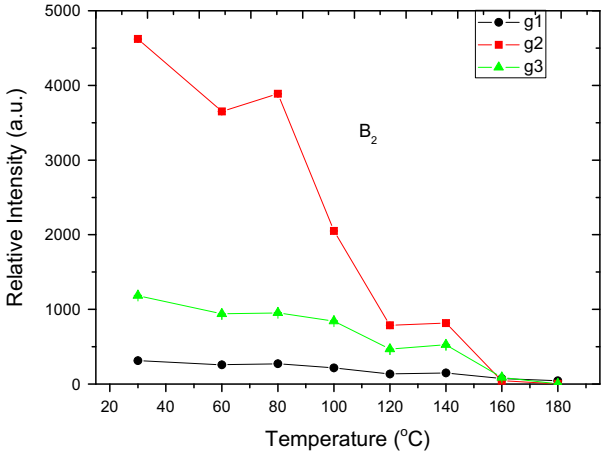

Fig. 9. Isochronal thermal treatment curve of the sample B_2 EPR responses.

After Houde-Walter et al. [14,15] the interdiffusion of the cations in glass is strongly dependent on the NBOs concentration.

Considering a tellurite glasses silver-doped glass sample submitted to the TT, the following effects are expected, which contribute to the formation of the precursor Ag^0 of the precipitation of metallic silver nanoparticles:

(a) the glass lattice degenerates with NBOs covalent bond breaking, releasing one O^{2-} ion per each broken bond (Fig. 14a),

(b) the released O^{2-} ion gives one electron to the diluted silver ion Ag^+ after the reaction $Ag^+ + O^{2-} \rightarrow Ag^0 + O^-$ (see Fig. 14b),

(c) the O^- ion will occupy an interstitial position, compensating the charge of an oxygen vacancy which was previously formed in the melt. After further TTs, the metallic silver nanoparticles may create a film on the glass sample surface after the Ag^0 diffusion, agglomeration and nucleation (see Fig. 14c),

(d) the NBO^- whose charge was previously compensated by the Ag^+ is now compensated by a neighboring oxygen vacancy V_O^+ (see Fig. 14c).

From the silver plasmon band wavelength localization, as compared with the results found in the literature [16], it is clear that the nanoparticles shape is spherical, as confirmed by our observations by TEM.

Due to the Zn presence in the chemical composition of sample B_1, after an initial nonradiative decay for the initial range of TT between 30 °C and 60 °C i.e. the phase (I), due to the reaction

$$NBOHC^0 + TeEC^0 \rightarrow NBO^- + V_O^+ \quad (1)$$

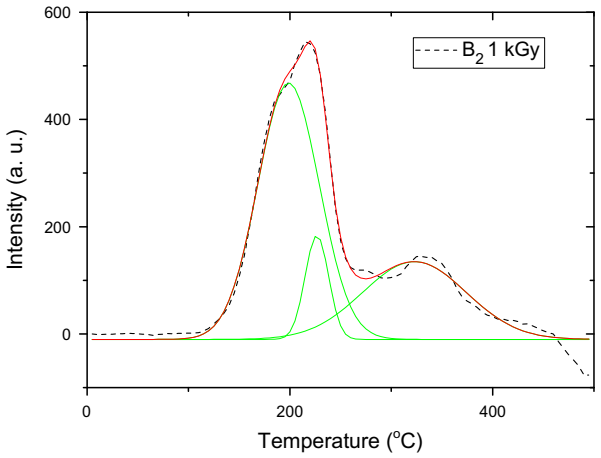

Fig. 12. TL glow curve of the sample B_2 irradiated with dose 1 kGy.

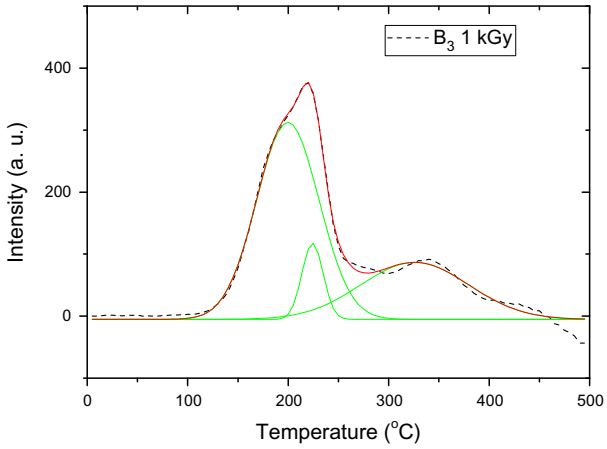

Fig. 13. TL glow curve of the sample B_3 irradiated with dose 1 kGy.

Table 6
Activation energy and TL peak positions (°C).

Sample (1 KGy)	Activation energy (eV)	1st peak (°C)	2nd peak (°C)	3rd peak (°C)
B_2	(0.90 ± 0.02)	195	223	326
B_1	(1.11 ± 0.02)	176	220	380
B_3	(1.03 ± 0.02)	198	224	325

At the further phase (II), starting the TT from 60 °C the curves reached a maximum at 80 °C, followed by a rapid decay until TT at 100 °C at the phase (III), and then the intensities continued the monotonical decrease similar to the initial decay at the phase (IV), similar to the initial decay. The complete extinction of $NBOHC^0$ and $TeEC^0$ is reached by the TT at a140 °C. The thermoluminescent emission (TL) appears only at temperatures higher than 130 °C. The higher TL intensity was observed for the sample B_2, indicating the presence of at least one nonparamagnetic center (which is not detected by EPR) responsible by the TL observed at higher temperature range than it was expected. Such conditions led us to the proposal of the following hypothesis of possible charge transfer mechanisms involved in the processes of irradiation and TT, as explained below.

Considering the highly probable situation of a Zn^{2+} occupying an interstitial glass modifying position in the glass matrix, compensating the charge of a couple of adjacent NBÓs, as indicated

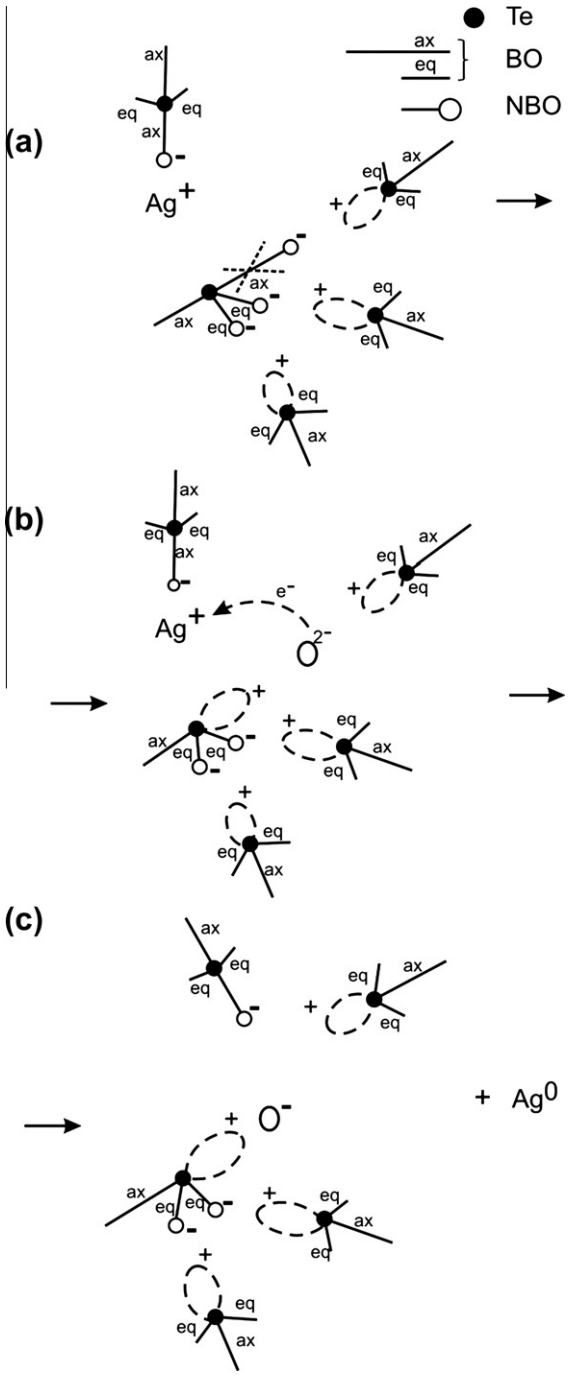

Fig. 14. Model of the formation of the Ag^0 precursor of metallic silver nanoparticles.

in Fig. 15, at the neighborhood of a pair (NBO^-, V_O^+) where an oxygen vacancy is charge-compensating a third NBO^- belonging to the same bipyramidal structural unit of the tellurite glass. On irradiation, the electrons released from a pair of neighboring NBÓs are trapped by the Zn^{2+} ion, leaving a pair of NBOHCs and Zn^0. During the TT between 30 °C and 60 °C, in the phase I, the pair of NBOHĆs becomes nonparamagnetic by means of the transference of an electron from one to the other, forming a valence alternate pair (NBO^-, $NBOHC^+$), where the $NBOHC^+$ has trapped two holes. In the next phases of the TT, the Zn^0 atom gives two electrons to the nearby oxygen vacancy in a process of two steps:

$$Zn^0 + V_0^+ \overset{TT(60-80\ ^\circ C)}{\rightarrow} Zn^+ + TeEC^0 \quad (2)$$

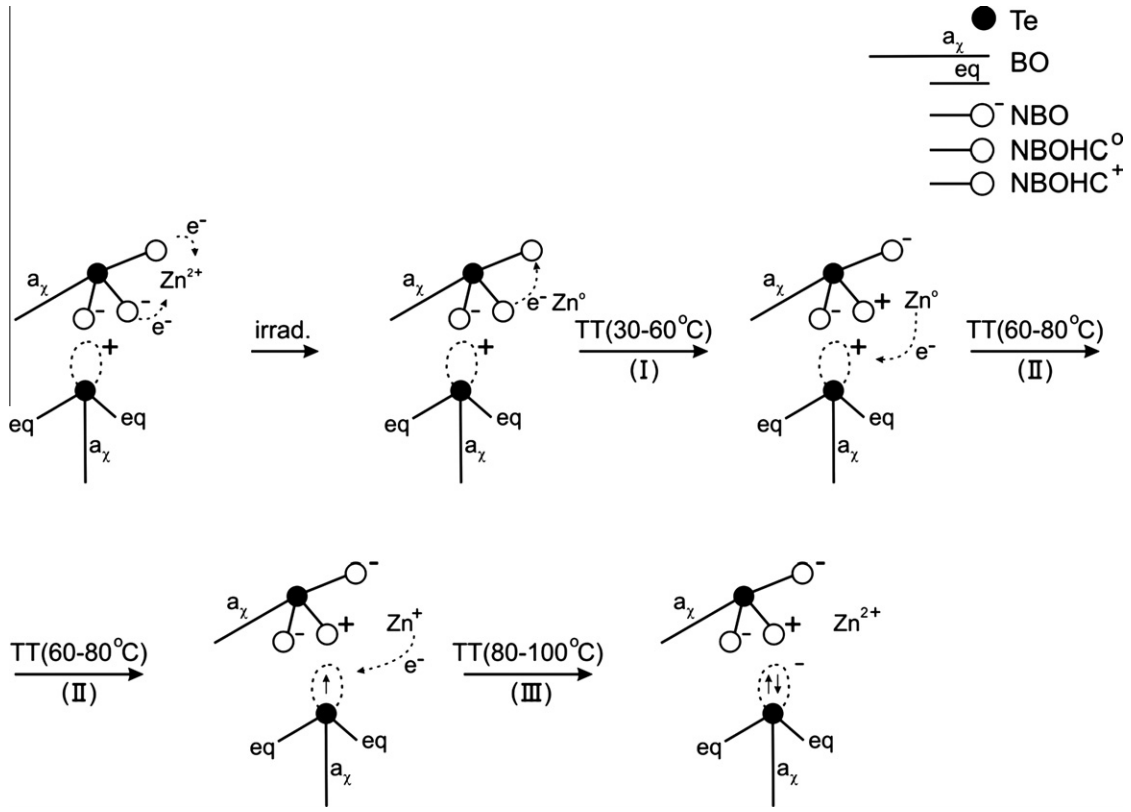

Fig. 15. Mechanism of the $TeEC^-$ formation on irradiation. The band notation is merely schematic.

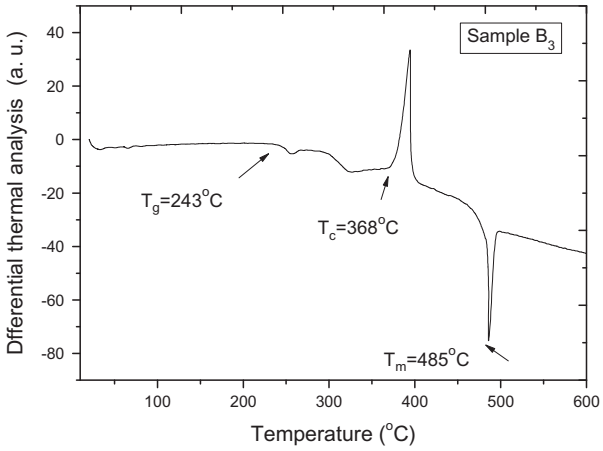

Fig. 16. DTA curve of the sample B_3.

$$Zn^+ + TeEC^0 \overset{TT(80-100\ ^\circ C)}{\rightarrow} Zn^{2+} + TeEC^- \quad (3)$$

At the phase (II) of 80 °C ⩽ TT ⩽ 100 °C occurs the growth of the $TeEC^0$, identified as the paramagnetic response at g_3. Next, in the phase (III), while the $TeEC^0$ starts to receive a second electron, the oxygen vacancy dangling orbital is going to be filled with two electrons giving rise to the $TeEC^-$, with paired spins, so that the EPR signal of g_3 starts to decrease. The completely filled dangling orbital of the $TeEC^-$ makes this center more stable than the $TeEC^0$, so that it survives up to the temperatures ⩾130 °C where the TL emission is observed. As the sample B_3 glass composition also contains Na^+ compensating the charge of a NBO^-, the thermal decay of the phase (IV) in the interval 100 °C ⩽ TT ⩽ 140 °C can be assigned to the same reaction observed at the phase (I):

$$NBOHC^0 + TeEC^- \rightarrow NBO^- + V_0^+ \quad (4)$$

The first TL peak is attributed to the nonparamagnetic center $TeEC^-$, whose proposal of the production mechanism on irradiation is illustrated in Fig. 15. The second peak is ascribed to the recombination of the residual TeOHC with deeper electrons, probably trapped by impurities. Finally, the third peak is due probably to the phenomena related with the powder synterization process. It occurs in the temperature range between Tg and Tc, characterized by a sudden negative (endothermic) fall in DTA, as a result of the energy release which occurs during the grain coalescence. In the case of a radiative energy release we can expect a TL peak at this temperature, which was effectively observed at 340 °C (see Fig. 16).

From the isochronal TT decay results (Figs. 8–10) and from the TL curves it is concluded that the recombination between the defect centers identified by the EPR responses at g_1, g_2 and g_3 is nonradiative.

The first TL peak is attributed to the radiative recombination of $TeEC^-$ (whose production is illustrated in Fig. 15) with a neighboring hole center. Using the initial slope method, the activation energy of the first TL peak, attributed for the $TeEC^-$ for the samples B_1, B_2 and B_3 are shown in Table 6. The TL peak positions for the samples B_1, B_2 and B_3 are shown in Table 6.

5. Conclusion

The precipitation of silver metal and/or oxide nanoparticles in thermally treated tellurite glasses doped with $AgNO_3$ occurred at the sample surface, rather than the bulk.

In the glass doped with low content of silver (0.5 mol% of $AgNO_3$), the number of nearly spherical silver nanoparticles has increased by nucleation under thermal treatment up to 290 °C. Conversely, the glass doped with high content of silver (5 mol% de $AgNO_3$) the nanoparticles examined after thermal treatment at

290 °C were already grown up to a limiting size, as inferred from the absence of the OA red shift and the higher wavelength value of the silver plasmon resonance.

A model was proposed for the silver nanoparticles precipitation mechanism produced by heat treatments, what depends on the presence of NBO's in the glass matrix, which are the sources of the negative oxygen ions responsible for the reduction of Ag^+ ions to neutral silver.

The radiation induced defect centers NBOHC and TeEC recombined non-radioactively up to the temperature of 140 °C, so that the first radiative recombination starting at the first TL initial slope at ~150 °C is attributed to the nonparamagnetic center $TeEC^-$ and TeOHC. The first TL peak is attributed to the radiative recombination of $TeEC^-$. The second peak is ascribed to the recombination of the residual TeOHC with deeper electrons, probably trapped by impurities. Finally, the third peak is due probably to the phenomena related with the powder synterization process.

Acknowledgement

The authors grateful to the Brazilian Agency Fundação de Apoio à Pesquisa do Estado de São Paulo (FAPESP) for the financial support.

References

[1] T. Yano, A. Watanabe, J. Appl. Phys. 42 (1971) 3674.
[2] W.M. Pontuschka, L.C. Barbosa, in: G. Lucovsky, M.A. Popescu (Eds.), Non-Crystalline Materials for Optoelectronics, INOE Publishing House, Bucharest, 2004, pp. 363–392.
[3] S. Tanabe, J. Alloys Compd. 675 (2006) 408.
[4] D.K. Durga, P. Yadagiri Reddy, N. Veeraiah, J. Lumin. 99 (2002) 53.
[5] G. Venkateswara Rao, N. Veeraiah, P. Yadagiri Reddy, Opt. Mater. 22 (2003) 295.
[6] G. Venkateswara Rao, P. Yadagiri Reddy, N. Veeraiah, Mater. Lett. 57 (2002) 403.
[7] V.K. Rai, L.S. Menezes, C.B. Araújo, L.R.P. Kassab, D.M. da Silva, R.A. Kobayashi, J. Appl. Phys. 103 (2008). 093526-1.
[8] M. Yamane, Y. Asahara, Glasses for Photonics, Cambridge University Press, Cambridge, 2000.
[9] C. Strohhöfer, A. Polman, J. Appl. Phys. 81 (2000) 1414.
[10] L.R.P. Kassab, C.B. de Araújo, R.A. Kobayashi, R.A. Pinto, D.M. da Silva, J. Appl. Phys. 102 (2007) 103515.
[11] J.Ph. Blondeau, F. Catan, C. Andreazza-Vignolle, N. Sbai, Plasmonics 3 (2008) 65.
[12] K. Terashima, S.H. Kim, T. Yoko, J. Am. Ceram. Soc. 78 (1995) 1601.
[13] J.M. Giehl, W.M. Pontuschka, L.C. Barbosa, Z.M.C. Ludwig, J. Non-Cryst. Solids 356 (2010) 1762.
[14] S.N. Houde-Walter, J.M. Inman, A.J. Dent, G.N. Greaves, J. Phys. Chem. 97 (1993) 9330.
[15] B. Messerschmidt, B.L. McIntire, S.N. Houde-Walter, J. Appl. Opt. 35 (1996) 5670.
[16] J.J. Mock, M. Barbic, D.R. Smith, S. Schultz, J. Chem. Phys. 116 (2002) 6755.